

# FastGAN

## TOWARDS FASTER AND STABILIZED GAN TRAINING FOR HIGH-FIDELITY FEW-SHOT IMAGE SYNTHESIS

**Bingchen Liu<sup>1,2</sup>, Yizhe Zhu<sup>2</sup>, Kunpeng Song<sup>1,2</sup>, Ahmed Elgammal<sup>1,2</sup>**

<sup>1</sup>Playform - Artrendex Inc., USA

<sup>2</sup>Department of Computer Science, Rutgers University

{bingchen.liu,yizhe.zhu,kunpeng.song}@rutgers.edu

elgammal@artrendex.com

### ABSTRACT

Training Generative Adversarial Networks (GAN) on high-fidelity images usually requires large-scale GPU-clusters and a vast number of training images. In this paper, we study the few-shot image synthesis task for GAN with minimum computing cost. We propose a light-weight GAN structure that gains superior quality on  $1024 \times 1024$  resolution. Notably, the model converges from scratch with just a few hours of training on a single RTX-2080 GPU, and has a consistent performance, even with less than 100 training samples. Two technique designs constitute our work, a skip-layer channel-wise excitation module and a self-supervised discriminator trained as a feature-encoder. With thirteen datasets covering a wide variety of image domains<sup>1</sup>, we show our model’s superior performance compared to the state-of-the-art StyleGAN2, when data and computing budget are limited.

### 1 INTRODUCTION

The fascinating ability to synthesize images using the state-of-the-art (SOTA) Generative Adversarial Networks (GANs) (Goodfellow et al., 2014) display a great potential of GANs for many intriguing real-life applications, such as image translation, photo editing, and artistic creation. However, expensive computing cost and the vast amount of required training data limit these SOTAs in real applications with only small image sets and low computing budgets.

In real-life scenarios, the available samples to train a GAN can be minimal, such as the medical images of a rare disease, a particular celebrity’s portrait set, and a specific artist’s artworks. Transfer-learning with a pre-trained model (Mo et al., 2020; Wang et al., 2020) is one solution for the lack of training images. Nevertheless, there is no guarantee to find a compatible pre-training dataset. Furthermore, if not, fine-tuning probably leads to even worse performance (Zhao et al., 2020).



Figure 1: **Synthetic results on  $1024^2$  resolution** of our model, trained from scratch on single RTX 2080-Ti GPU, with only 1000 images. Left: 20 hours on Nature photos; Right: 10 hours on FFHQ.

In a recent study, it was highlighted that in art creation applications, most artists prefers to train their models from scratch based on their own images to avoid biases from fine-tuned pre-trained model.

<sup>1</sup>The datasets and code are available at: <https://github.com/odegasslbc/FastGAN-pytorch>

Moreover, it was shown that in most cases artists want to train their models with datasets of less than 100 images (Elgammal et al., 2020). Dynamic data-augmentation (Karras et al., 2020a; Zhao et al., 2020) smooths the gap and stabilizes GAN training with fewer images. However, the computing cost from the SOTA models such as StyleGAN2 (Karras et al., 2020b) and BigGAN (Brock et al., 2018) remain to be high, especially when trained with the image resolution on  $1024 \times 1024$ .

In this paper, our goal is to learn an unconditional GAN on high-resolution images, with low computational cost and few training samples. As summarized in Fig. 2, these training conditions expose the model to a high risk of overfitting and mode-collapse (Arjovsky & Bottou, 2017; Zhang & Khoreva, 2018). To train a GAN given the demanding training conditions, we need a generator  $G$  that can learn fast, and a discriminator  $D$  that can continuously provide useful signals to train  $G$ . To address these challenges, we summarize our contribution as:

- ✓ We design the Skip-Layer channel-wise Excitation (SLE) module, which leverages low-scale activations to revise the channel responses on high-scale feature-maps. SLE allows a more robust gradient flow throughout the model weights for faster training. It also leads to an automated learning of a style/content disentanglement like StyleGAN2.
- ✓ We propose a self-supervised discriminator  $D$  trained as a feature-encoder with an extra decoder. We force  $D$  to learn a more descriptive feature-map covering more regions from an input image, thus yielding more comprehensive signals to train  $G$ . We test multiple self-supervision strategies for  $D$ , among which we show that auto-encoding works the best.
- ✓ We build a computational-efficient GAN model based on the two proposed techniques, and show the model’s robustness on multiple high-fidelity datasets, as demonstrated in Fig. 1.

## 2 RELATED WORKS

**Speed up the GAN training:** Speeding up the training of GAN has been approached from various perspectives. Ngxande et al. propose to reduce the computing time with depth-wise convolutions. Zhong et al. adjust the GAN objective into a min-max-min problem for a shorter optimization path. Sinha et al. suggest to prepare each batch of training samples via a core-set selection, leverage the better data preparation for a faster convergence. However, these methods only bring a limited improvement in training speed. Moreover, the synthesis quality is not advanced within the shortened training time.

**Train GAN on high resolution:** High-resolution training for GAN can be problematic. Firstly, the increased model parameters lead to a more rigid gradient flow to optimize  $G$ . Secondly, the target distribution formed by the images on  $1024 \times 1024$  resolution is super sparse, making GAN much harder to converge. Denton et al. (2015); Zhang et al. (2017); Huang et al. (2017); Wang et al. (2018); Karras et al. (2019); Karnewar & Wang (2019); Karras et al. (2020b); Liu et al. (2020a) develop the multi-scale GAN structures to alleviate the gradient flow issue, where  $G$  outputs images and receives feedback from several resolutions simultaneously. However, all these approaches further increase the computational cost, consuming even more GPU memory and training time.

**Stabilize the GAN training:** Mode-collapse on  $G$  is one of the big challenges when training GANs. And it becomes even more challenging given fewer training samples and a lower computational budget (a smaller batch-size). As  $D$  is more likely to be overfitting on the datasets, thus unable to provide meaningful gradients to train  $G$  (Gulrajani et al., 2017).

Prior works tackle the overfitting issue by seeking a good regularization for  $D$ , including different objectives (Arjovsky et al., 2017; Lim & Ye, 2017; Tran et al., 2017); regularizing the gradients (Gulrajani et al., 2017; Mescheder et al., 2018); normalizing the model weights (Miyato et al., 2018); and augmenting the training data (Karras et al., 2020a; Zhao et al., 2020). However, the effects of these methods degrade fast when the training batch-size is limited, since appropriate batch statistics can hardly be calculated for the regularization (normalization) over the training iterations.

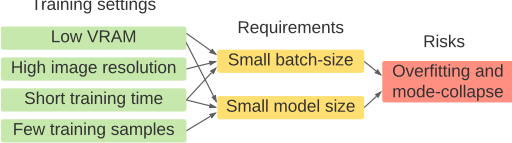


Figure 2: The causes and challenges for training GAN in our studied conditions.



along the spatial-dimensions, then a conv-layer further down-samples it into  $1 \times 1$ . A LeakyReLU is used to model the non-linearity, and another conv-layer projects  $\mathbf{x}_{low}$  to have the same channel size as  $\mathbf{x}_{high}$ . Finally, after a gating operation via a Sigmoid function, the output from  $\mathcal{F}$  multiplies  $\mathbf{x}_{high}$  along the channel dimension, yielding  $\mathbf{y}$  with the same shape as  $\mathbf{x}_{high}$ .

SLE partially resembles the Squeeze-and-Excitation module (SE) proposed by Hu et al.. However, SLE operates within one feature-map as a self-gating module. In comparison, SLE performs between feature-maps that are far away from each other. While SLE brings the benefit of channel-wise feature re-calibration just like SE, it also strengthens the whole model’s gradient flow like ResBlock. The channel-wise multiplication in SLE also coincides with Instance Normalization (Ulyanov et al., 2016; Huang & Belongie, 2017), which is widely used in style-transfer. Similarly, we show that SLE enables  $G$  to automatically disentangle the content and style attributes, just like StyleGAN (Karras et al., 2019). As SLE performs on high-resolution feature-maps, altering these feature-maps is shown to be more likely to change the style attributes of the generated image (Karras et al., 2019; Liu et al., 2020a). By replacing  $\mathbf{x}_{low}$  in SLE from another synthesized sample, our  $G$  can generate an image with the content unchanged, but in the same style of the new replacing image.

### 3.2 SELF-SUPERVISED DISCRIMINATOR

Our approach to provide a strong regularization for  $D$  is surprisingly simple. We treat  $D$  as an encoder and train it with small decoders. Such auto-encoding training forces  $D$  to extract image features that the decoders can give good reconstructions. The decoders are optimized together with  $D$  on a simple reconstruction loss, which is only trained on real samples:

$$\mathcal{L}_{recons} = \mathbb{E}_{\mathbf{f} \sim D_{encode}(x), x \sim I_{real}} [||\mathcal{G}(\mathbf{f}) - \mathcal{T}(x)||], \quad (2)$$

where  $\mathbf{f}$  is the intermediate feature-maps from  $D$ , the function  $\mathcal{G}$  contains the processing on  $\mathbf{f}$  and the decoder, and the function  $\mathcal{T}$  represents the processing on sample  $x$  from real images  $I_{real}$ .

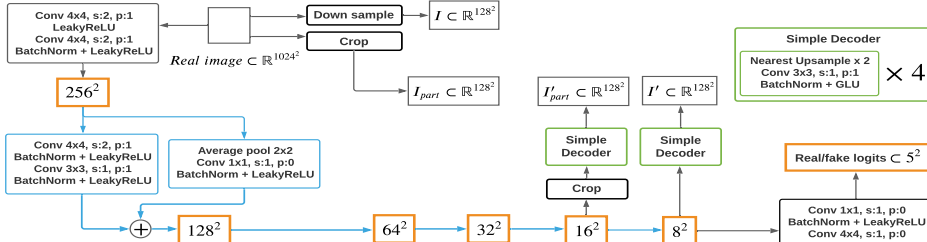


Figure 4: The structure and the forward flow of the Discriminator. Blue box and arrows represent the same residual down-sampling structure, green boxes mean the same decoder structure.

Our self-supervised  $D$  is illustrated in Fig. 4, where we employ two decoders for the feature-maps on two scales:  $\mathbf{f}_1$  on  $16^2$  and  $\mathbf{f}_2$  on  $8^2$ . The decoders only have four conv-layers to produce images at  $128 \times 128$  resolution, causing little extra computations (much less than other regularization methods). We randomly crop  $\mathbf{f}_1$  with  $\frac{1}{8}$  of its height and width, then crop the real image on the same portion to get  $I_{part}$ . We resize the real image to get  $I$ . The decoders produce  $I'_{part}$  from the cropped  $\mathbf{f}_1$ , and  $I'$  from  $\mathbf{f}_2$ . Finally,  $D$  and the decoders are trained together to minimize the loss in eq. 2, by matching  $I'_{part}$  to  $I_{part}$  and  $I'$  to  $I$ .

Such reconstructive training makes sure that  $D$  extracts a more comprehensive representation from the inputs, covering both the overall compositions (from  $\mathbf{f}_2$ ) and detailed textures (from  $\mathbf{f}_1$ ). Note that the processing in  $\mathcal{G}$  and  $\mathcal{T}$  are not limited to cropping; more operations remain to be explored for better performance. The auto-encoding approach we employ is a typical method for self-supervised learning, which has been well recognized to improve the model robustness and generalization ability (He et al., 2020; Hendrycks et al., 2019; Jing & Tian, 2020; Goyal et al., 2019). In the context of GAN, we find that a regularized  $D$  via self-supervision training strategies significantly improves the synthesis quality on  $G$ , among which auto-encoding brings the most performance boost.

Although our self-supervision strategy for  $D$  comes in the form of an auto-encoder (AE), this approach is fundamentally different from works trying to combine GAN and AE (Larsen et al., 2016;

Guo et al., 2019; Zhao et al., 2016; Berthelot et al., 2017). The latter works mostly train  $G$  as a decoder on a learned latent space from  $D$ , or treat the adversarial training with  $D$  as an supplementary loss besides AE’s training. In contrast, our model is a pure GAN with a much simpler training schema. The auto-encoding training is only for regularizing  $D$ , where  $G$  is not involved.

Hinge Loss computes  
the fastest.

In sum, we employ the hinge version of the adversarial loss (Lim & Ye (2017); Tran et al. (2017)) to iteratively train our  $D$  and  $G$ . We find the different GAN losses make little performance difference, while hinge loss computes the fastest:

$$\mathcal{L}_D = -\mathbb{E}_{x \sim I_{real}}[\min(0, -1 + D(x))] - \mathbb{E}_{\hat{x} \sim G(z)}[\min(0, -1 - D(\hat{x})] + \mathcal{L}_{recons} \quad (3)$$

$$\mathcal{L}_G = -\mathbb{E}_{z \sim \mathcal{N}}[D(G(z))], \quad (4)$$

## 4 EXPERIMENT

**Datasets:** We conduct experiments on multiple datasets with a wide range of content categories. On  $256 \times 256$  resolution, we test on Animal-Face Dog and Cat (Si & Zhu, 2011), 100-Shot-Obama, Panda, and Grumpy-cat (Zhao et al., 2020). On  $1024 \times 1024$  resolution, we test on Flickr-Face-HQ (FFHQ) (Karras et al., 2019), Oxford-flowers (Nilsback & Zisserman, 2006), art paintings from WikiArt (wikiart.org), photographs on natural landscape from Unsplash (unsplash.com), Pokemon (pokemon.com), anime face, skull, and shell. These datasets are designed to cover images with different characteristics: photo realistic, graphic-illustration, and art-like images.

**Metrics:** We use two metrics to measure the models’ synthesis performance: 1) Fréchet Inception Distance (FID) (Heusel et al., 2017) measures the overall semantic realism of the synthesized images. For datasets with less than 1000 images (most only have 100 images), we let  $G$  generate 5000 images and compute FID between the synthesized images and the whole training set. 2) Learned perceptual similarity (LPIPS) (Zhang et al., 2018) provides a perceptual distance between two images. We use LPIPS to report the reconstruction quality when we perform latent space back-tracking on  $G$  given real images, and measure the auto-encoding performance. We find it unnecessary to involve other metrics, as FID is unlikely to be inconsistent with the others, given the notable performance gap between our model and the compared ones. For all the testings, we train the models 5 times with random seeds, and report the highest scores. The relative error is less than five percent on average.

**Compared Models:** We compare our model with: 1) the state-of-the-art (SOTA) unconditional model, StyleGAN2, 2) a baseline model ablated from our proposed one. Note that we adopt StyleGAN2 with recent studies from (Karras et al., 2020a; Zhao et al., 2020), including the model configuration and differentiable data-augmentation, for the best training on few-sample datasets. Since StyleGAN2 requires much more computing-cost (cc) to train, we derive an extra baseline model. In sum, we compare our model with StyleGAN2 on the absolute image synthesis quality regardless of cc, and use the baseline model for the reference within a comparable cc range.

The baseline model is the strongest performer that we integrated from various GAN techniques based on DCGAN (Radford et al., 2015): 1) spectral-normalization (Miyato et al., 2018), 2) exponential-moving-average (Yazıcı et al., 2018) optimization on  $G$ , 3) differentiable-augmentation, 4) GLU (Dauphin et al., 2017) instead of ReLU in  $G$ . We build our model upon the baseline with the two proposed techniques: the skip-layer excitation module and the self-supervised discriminator.

Table 1: Computational cost comparison of the models.

		StyleGAN2@0.25	StyleGAN2@0.5	StyleGAN2	Baseline	Ours
Resolution: $256^2$	Training time (hour / 10k iter)	1	1.8	3.8	0.7	1
Batch-size: 8	Training vram (GB)	7	16	18	5	6.5
	Model parameters (million)	27.557	45.029	108.843	44.359	47.363
Resolution: $1024^2$	Training time (hour / 10k iter)	3.6	5	7	1.3	1.7
Batch-size: 8	Training vram (GB)	12	23	36	9	10
	Model parameters (million)	27.591	45.15	109.229	44.377	47.413

Table. 1 presents the normalized cc figures of the models on Nvidia’s RTX 2080-Ti GPU, implemented using PyTorch (Paszke et al., 2017). Importantly, the slimed StyleGAN2 with  $\frac{1}{4}$  parameters





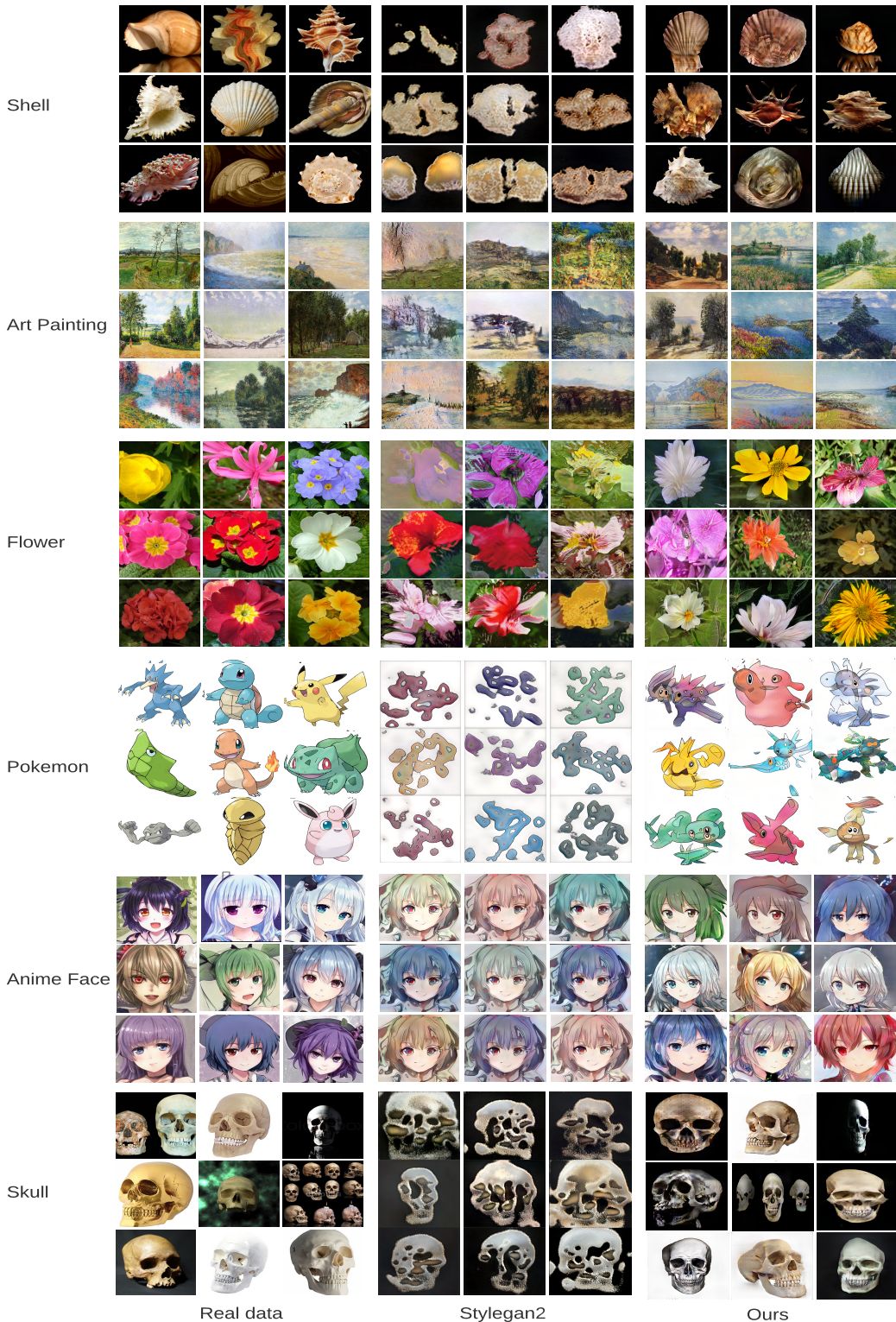


Figure 6: **Qualitative comparison between our model and StyleGAN2** on  $1024^2$  resolution datasets. The left-most panel shows the training images, and the right two panels show the uncurated samples from StyleGAN2 and our model. Both models are trained from scratch for 10 hours with a batch-size of 8. The samples are generated from the checkpoint with the lowest FID.

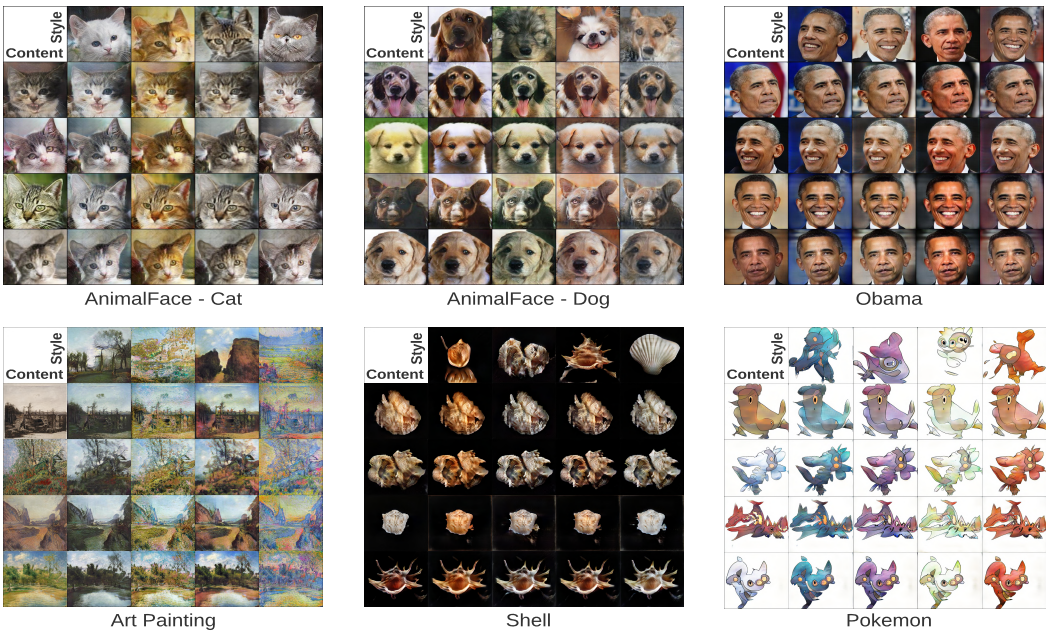


Figure 7: Style-mixing results from our model trained for only 5 hours on single GPU.

their inversions from  $G$ , after the same update of 1000 iterations on the latent vectors (to prevent the vectors from being far off the normal distribution). The baseline model’s performance is getting worse with more training iterations, which reflects mode-collapse on  $G$ . In contrast, our model gives better reconstructions with consistent performance over more training iterations. Fig. 5 presents the back-tracked examples (left-most and right-most samples in the middle panel) given the real images. The smooth interpolations from the back-tracked latent vectors also suggest little mode-collapse of our  $G$  (Radford et al., 2015; Zhao et al., 2020; Robb et al., 2020).

In addition, we show qualitative comparisons in appendix D, where our model maintains a good generation while StyleGAN2 and baseline are model-collapsed.

**The self-supervision methods and generalization ability on  $D$ :** Apart from the auto-encoding training for  $D$ , we show that  $D$  with other common self-supervising strategies also boost GAN’s performance in our training settings. We test five self-supervision settings, as shown in Table 6, which all brings a substantial performance boost compared to the baseline model. Specifically, setting-a refers to contrastive learning which we treat each real image as a unique class and let  $D$  classify them. For setting-b, we train  $D$  to predict the real image’s original aspect-ratio since they are reshaped to square when fed to  $D$ . Setting-c is the method we employ in our model, which trains  $D$  as an encoder with a decoder to reconstruct real images. To better validate the benefit of self-supervision on  $D$ , all the testings are conducted on full training sets with 10000 images, with a batch-size of 8 to be consistent with Table 4. We also tried training with a larger batch-size of 16, which the results are consistent to the batch-size of 8.

Interestingly, according to Table 6, while setting-c performs the best, combining it with the rest two settings lead to a clear performance downgrade. The similar behavior can be found on some other self-supervision settings, e.g. when follow Chen et al. (2019) with a “rotation-predicting” task on art-paintings and FFHQ datasets, we observe a performance downgrade even compared to the baseline model. We hypothesis the reason being that the auto-encoding forces  $D$  to pay attention to more areas of the input image, thus extracts a more comprehensive feature-map to describe the input image (for a good reconstruction). In contrast, a classification task does not guarantee  $D$  to cover the whole image. Instead, the task drives  $D$  to only focus on small regions because the model can find class cues from small regions of the images. Focusing on limited regions (i.e., react to limited image patterns) is a typical overfitting behavior, which is also widely happening for  $D$  in vanilla GANs. More discussion can be found in appendix B.

**Style mixing like StyleGAN.** With the channel-wise excitation module, our model gets the same functionality as StyleGAN: it learns to disentangle the images’ high-level semantic attributes (style and content) in an unsupervised way, from  $G$ ’s conv-layers at different scales. The style-mixing results are displayed in Fig. 7, where the top three datasets are  $256 \times 256$  resolution, and the bottom three are  $1024 \times 1024$  resolution. While StyleGAN2 suffers from converging on the bottom high-resolution datasets, our model successfully learns the style representations along the channel dimension on the “excited” layers (i.e., for feature-maps on  $256 \times 256$ ,  $512 \times 512$  resolution). Please refer to appendix A and C for more information on SLE and style-mixing.

## 5 CONCLUSION

We introduce two techniques that stabilize the GAN training with an improved synthesis quality, given sub-hundred high-fidelity images and a limited computing resource. On thirteen datasets with a diverse content variation, we show that a skip-layer channel-wise excitation mechanism (SLE) and a self-supervised regularization on the discriminator significantly boost the synthesis performance of GAN. Both proposed techniques require minor changes to a vanilla GAN, enhancing GAN’s practicality with a desirable plug-and-play property. We hope this work can benefit downstream tasks of GAN (Liu et al., 2020c;b; Elgammal et al., 2017) and provide new study perspectives for future research.

## REFERENCES

- Rameen Abdal, Yipeng Qin, and Peter Wonka. Image2stylegan: How to embed images into the stylegan latent space? In *Proceedings of the IEEE international conference on computer vision*, pp. 4432–4441, 2019.
- Martin Arjovsky and Leon Bottou. Towards principled methods for training generative adversarial networks. *arXiv preprint arXiv:1701.04862*, 2017.
- Martin Arjovsky, Soumith Chintala, and Leon Bottou. Wasserstein gan, 2017.
- David Berthelot, Thomas Schumm, and Luke Metz.Began: Boundary equilibrium generative adversarial networks. *arXiv preprint arXiv:1703.10717*, 2017.
- Andrew Brock, Jeff Donahue, and Karen Simonyan. Large scale gan training for high fidelity natural image synthesis. *arXiv preprint arXiv:1809.11096*, 2018.
- Ting Chen, Xiaohua Zhai, Marvin Ritter, Mario Lucic, and Neil Houlsby. Self-supervised gans via auxiliary rotation loss. In *Proceedings of the IEEE Conference on Computer Vision and Pattern Recognition*, pp. 12154–12163, 2019.
- Yann N Dauphin, Angela Fan, Michael Auli, and David Grangier. Language modeling with gated convolutional networks. In *International conference on machine learning*, pp. 933–941, 2017.
- Emily L Denton, Soumith Chintala, Rob Fergus, et al. Deep generative image models using a laplacian pyramid of adversarial networks. In *Advances in neural information processing systems*, pp. 1486–1494, 2015.
- Ahmed Elgammal, Bingchen Liu, Mohamed Elhoseiny, and Marian Mazzone. Can: Creative adversarial networks, generating “art” by learning about styles and deviating from style norms. *arXiv preprint arXiv:1706.07068*, 2017.
- Ahmed Elgammal, Marian Mazzone, et al. Artists, artificial intelligence and machine-based creativity in playform. *Artnodes*, (26):1–8, 2020.
- Ian Goodfellow, Jean Pouget-Abadie, Mehdi Mirza, Bing Xu, David Warde-Farley, Sherjil Ozair, Aaron Courville, and Yoshua Bengio. Generative adversarial nets. In *Advances in neural information processing systems*, pp. 2672–2680, 2014.
- Priya Goyal, Dhruv Mahajan, Abhinav Gupta, and Ishan Misra. Scaling and benchmarking self-supervised visual representation learning. In *Proceedings of the IEEE International Conference on Computer Vision*, pp. 6391–6400, 2019.

- Ishaan Gulrajani, Faruk Ahmed, Martin Arjovsky, Vincent Dumoulin, and Aaron C Courville. Improved training of wasserstein gans. In *Advances in neural information processing systems*, pp. 5767–5777, 2017.
- Yong Guo, Qi Chen, Jian Chen, Qingyao Wu, Qinfeng Shi, and Mingkui Tan. Auto-embedding generative adversarial networks for high resolution image synthesis. *IEEE Transactions on Multimedia*, 21(11):2726–2737, 2019.
- Kaiming He, Xiangyu Zhang, Shaoqing Ren, and Jian Sun. Deep residual learning for image recognition. In *Proceedings of the IEEE conference on computer vision and pattern recognition*, pp. 770–778, 2016.
- Kaiming He, Haoqi Fan, Yuxin Wu, Saining Xie, and Ross Girshick. Momentum contrast for unsupervised visual representation learning. In *Proceedings of the IEEE/CVF Conference on Computer Vision and Pattern Recognition*, pp. 9729–9738, 2020.
- Dan Hendrycks, Mantas Mazeika, Saurav Kadavath, and Dawn Song. Using self-supervised learning can improve model robustness and uncertainty. In *Advances in Neural Information Processing Systems*, pp. 15663–15674, 2019.
- Martin Heusel, Hubert Ramsauer, Thomas Unterthiner, Bernhard Nessler, and Sepp Hochreiter. Gans trained by a two time-scale update rule converge to a local nash equilibrium. In *Advances in neural information processing systems*, pp. 6626–6637, 2017.
- Jie Hu, Li Shen, and Gang Sun. Squeeze-and-excitation networks. In *Proceedings of the IEEE conference on computer vision and pattern recognition*, pp. 7132–7141, 2018.
- Xun Huang and Serge Belongie. Arbitrary style transfer in real-time with adaptive instance normalization. In *Proceedings of the IEEE International Conference on Computer Vision*, pp. 1501–1510, 2017.
- Xun Huang, Yixuan Li, Omid Poursaeed, John Hopcroft, and Serge Belongie. Stacked generative adversarial networks. In *Proceedings of the IEEE conference on computer vision and pattern recognition*, pp. 5077–5086, 2017.
- Longlong Jing and Yingli Tian. Self-supervised visual feature learning with deep neural networks: A survey. *IEEE Transactions on Pattern Analysis and Machine Intelligence*, 2020.
- Animesh Karnewar and Oliver Wang. Msg-gan: multi-scale gradient gan for stable image synthesis. *arXiv preprint arXiv:1903.06048*, 2019.
- Tero Karras, Timo Aila, Samuli Laine, and Jaakko Lehtinen. Progressive growing of gans for improved quality, stability, and variation. *arXiv preprint arXiv:1710.10196*, 2017.
- Tero Karras, Samuli Laine, and Timo Aila. A style-based generator architecture for generative adversarial networks. In *Proceedings of the IEEE conference on computer vision and pattern recognition*, pp. 4401–4410, 2019.
- Tero Karras, Miika Aittala, Janne Hellsten, Samuli Laine, Jaakko Lehtinen, and Timo Aila. Training generative adversarial networks with limited data. *arXiv preprint arXiv:2006.06676*, 2020a.
- Tero Karras, Samuli Laine, Miika Aittala, Janne Hellsten, Jaakko Lehtinen, and Timo Aila. Analyzing and improving the image quality of stylegan. In *Proceedings of the IEEE/CVF Conference on Computer Vision and Pattern Recognition*, pp. 8110–8119, 2020b.
- Anders Boesen Lindbo Larsen, Søren Kaae Sønderby, Hugo Larochelle, and Ole Winther. Autoencoding beyond pixels using a learned similarity metric. In *International conference on machine learning*, pp. 1558–1566. PMLR, 2016.
- Jae Hyun Lim and Jong Chul Ye. Geometric gan. *arXiv preprint arXiv:1705.02894*, 2017.
- Zachary C Lipton and Subarna Tripathi. Precise recovery of latent vectors from generative adversarial networks. *arXiv preprint arXiv:1702.04782*, 2017.

- Bingchen Liu, Kunpeng Song, Yizhe Zhu, Gerard de Melo, and Ahmed Elgammal. Time: Text and image mutual-translation adversarial networks. *arXiv preprint arXiv:2005.13192*, 2020a.
- Bingchen Liu, Kunpeng Song, Yizhe Zhu, and Ahmed Elgammal. Sketch-to-art: Synthesizing stylized art images from sketches. In *Proceedings of the Asian Conference on Computer Vision (ACCV)*, November 2020b.
- Bingchen Liu, Yizhe Zhu, Zuohui Fu, Gerard de Melo, and Ahmed Elgammal. Oogan: Disentangling gan with one-hot sampling and orthogonal regularization. 2020c.
- Lars Mescheder, Andreas Geiger, and Sebastian Nowozin. Which training methods for gans do actually converge? *arXiv preprint arXiv:1801.04406*, 2018.
- Takeru Miyato, Toshiki Kataoka, Masanori Koyama, and Yuichi Yoshida. Spectral normalization for generative adversarial networks. *arXiv preprint arXiv:1802.05957*, 2018.
- Sangwoo Mo, Minsu Cho, and Jinwoo Shin. Freeze discriminator: A simple baseline for fine-tuning gans. *arXiv preprint arXiv:2002.10964*, 2020.
- Mkhuseli Ngxande, Jules-Raymond Tapamo, and Michael Burke. Depthwisegans: Fast training generative adversarial networks for realistic image synthesis. In *2019 Southern African Universities Power Engineering Conference/Robotics and Mechatronics/Pattern Recognition Association of South Africa (SAUPEC/RobMech/PRASA)*, pp. 111–116. IEEE, 2019.
- Maria-Elena Nilsback and Andrew Zisserman. A visual vocabulary for flower classification. In *IEEE Conference on Computer Vision and Pattern Recognition*, volume 2, pp. 1447–1454, 2006.
- Atsuhiro Noguchi and Tatsuya Harada. Image generation from small datasets via batch statistics adaptation. In *Proceedings of the IEEE International Conference on Computer Vision*, pp. 2750–2758, 2019.
- Adam Paszke, Sam Gross, Soumith Chintala, Gregory Chanan, Edward Yang, Zachary DeVito, Zeming Lin, Alban Desmaison, Luca Antiga, and Adam Lerer. Automatic differentiation in pytorch. 2017.
- Alec Radford, Luke Metz, and Soumith Chintala. Unsupervised representation learning with deep convolutional generative adversarial networks. *arXiv preprint arXiv:1511.06434*, 2015.
- Esther Robb, Wen-Sheng Chu, Abhishek Kumar, and Jia-Bin Huang. Few-shot adaptation of generative adversarial networks. *arXiv preprint arXiv:2010.11943*, 2020.
- Zhangzhang Si and Song-Chun Zhu. Learning hybrid image templates (hit) by information projection. *IEEE Transactions on pattern analysis and machine intelligence*, 34(7):1354–1367, 2011.
- Samarth Sinha, Han Zhang, Anirudh Goyal, Yoshua Bengio, Hugo Larochelle, and Augustus Odena. Small-gan: Speeding up gan training using core-sets. *arXiv preprint arXiv:1910.13540*, 2019.
- Dustin Tran, Rajesh Ranganath, and David M Blei. Deep and hierarchical implicit models. *arXiv preprint arXiv:1702.08896*, 7(3):13, 2017.
- Ngoc-Trung Tran, Viet-Hung Tran, Bao-Ngoc Nguyen, Linxiao Yang, and Ngai-Man Man Cheung. Self-supervised gan: Analysis and improvement with multi-class minimax game. *Advances in Neural Information Processing Systems*, 32:13253–13264, 2019.
- Dmitry Ulyanov, Andrea Vedaldi, and Victor Lempitsky. Instance normalization: The missing ingredient for fast stylization. *arXiv preprint arXiv:1607.08022*, 2016.
- Ting-Chun Wang, Ming-Yu Liu, Jun-Yan Zhu, Andrew Tao, Jan Kautz, and Bryan Catanzaro. High-resolution image synthesis and semantic manipulation with conditional gans. In *Proceedings of the IEEE conference on computer vision and pattern recognition*, pp. 8798–8807, 2018.
- Yaxing Wang, Abel Gonzalez-Garcia, David Berga, Luis Herranz, Fahad Shahbaz Khan, and Joost van de Weijer. Minegan: effective knowledge transfer from gans to target domains with few images. In *Proceedings of the IEEE/CVF Conference on Computer Vision and Pattern Recognition*, pp. 9332–9341, 2020.

Yasin Yazıcı, Chuan-Sheng Foo, Stefan Winkler, Kim-Hui Yap, Georgios Piliouras, and Vijay Chandrasekhar. The unusual effectiveness of averaging in gan training. *arXiv preprint arXiv:1806.04498*, 2018.

Dan Zhang and Anna Khoreva. Pa-gan: Improving gan training by progressive augmentation. 2018.

Han Zhang, Tao Xu, Hongsheng Li, Shaoting Zhang, Xiaogang Wang, Xiaolei Huang, and Dimitris N Metaxas. Stackgan: Text to photo-realistic image synthesis with stacked generative adversarial networks. In *Proceedings of the IEEE international conference on computer vision*, pp. 5907–5915, 2017.

Richard Zhang, Phillip Isola, Alexei A Efros, Eli Shechtman, and Oliver Wang. The unreasonable effectiveness of deep features as a perceptual metric. In *Proceedings of the IEEE conference on computer vision and pattern recognition*, pp. 586–595, 2018.

Junbo Zhao, Michael Mathieu, and Yann LeCun. Energy-based generative adversarial network. *arXiv preprint arXiv:1609.03126*, 2016.

Shengyu Zhao, Zhijian Liu, Ji Lin, Jun-Yan Zhu, and Song Han. Differentiable augmentation for data-efficient gan training. *arXiv preprint arXiv:2006.10738*, 2020.

Jiachen Zhong, Xuanqing Liu, and Cho-Jui Hsieh. Improving the speed and quality of gan by adversarial training. *arXiv preprint arXiv:2008.03364*, 2020.

Jiapeng Zhu, Yujun Shen, Deli Zhao, and Bolei Zhou. In-domain gan inversion for real image editing. *arXiv preprint arXiv:2004.00049*, 2020.

Jun-Yan Zhu, Philipp Krähenbühl, Eli Shechtman, and Alexei A Efros. Generative visual manipulation on the natural image manifold. In *European conference on computer vision*, pp. 597–613. Springer, 2016.

## Appendix

### A PERFORMANCE BOOST FROM SKIP-LAYER EXCITATION

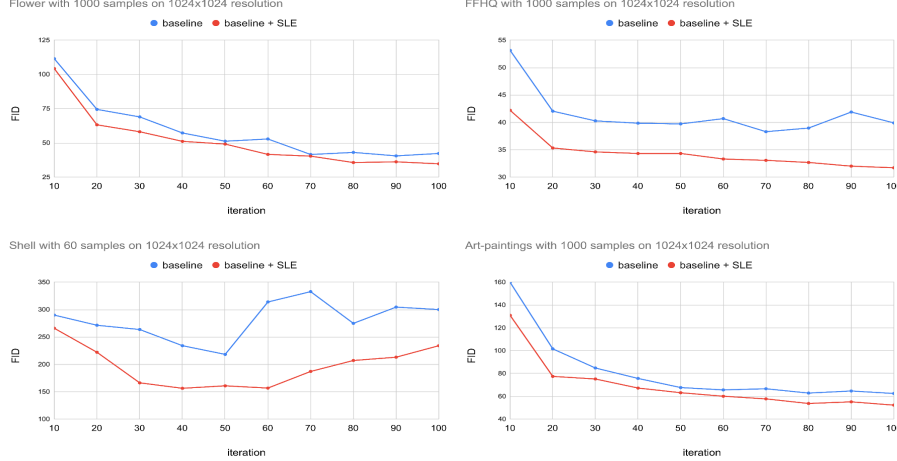


Figure 8: **Ablation study for SLE module** on  $1024 \times 1024$  resolution datasets. Each unit on the x-axis represents 1000 training iterations, and y-axis represents the FID score.

Here we present a more detailed ablation study for the skip-layer excitation (SLE) module. We compare between the baseline model and the baseline equipped with SLE. On four  $1024 \times 1024$  resolutions datasets: Flower, FFHQ, Shell and Art-paintings, we record the FID performance every 10000 iterations for every model. As shown in Fig. 8, SLE brings a constant performance boost on the baseline model over all iterations.

Our key observation is, SLE speeds up the convergence of GAN, where the most noticeable effect happens at the beginning of the training. In the first 20000 iterations, the generator  $G$  is able to converge faster and reach to a good point where the baseline model needs much more training iterations to reach. On the other hand, although SLE provides a faster convergence on  $G$ , the overall model behavior with SLE seems follow the baseline model quite well, with a slightly better overall performance.

In other words, the lines for the two models are parallel in each sub-plot in Fig. 8. Specifically, on Shell, the model with SLE also collapsed after 60000 iterations training, just like the baseline model. And on the rest three datasets, the FID improves much slower and almost stop changing in the later half training iterations. We think such model behavior makes sense, because the SLE module neither increases the model capacity (have very few parameter increase) nor exert any explicit regularization or guidance on the training of GAN. Therefore, SLE is unlikely to make a big difference after the model reaches a good converged state.

On the other hand, SLE does a good job speeding up the convergence for  $G$ , and improves the performance of  $G$ . More importantly, it is SLE that enables the unsupervised style-content disentanglement for our model, in a simpler and more cost-efficient way than StyleGAN and StyleGAN2.

### B FEATURE-EXTRACTION PERFORMANCE OF DISCRIMINATOR

Here we continue the discussion on the effectiveness of the self-supervised auto-encoding training for the discriminator  $D$ . Specifically, we explore the relationship between the *feature-extracting behavior on the discriminator  $D$*  and the *synthesis performance of GAN*. By feature-extracting performance, we mean how comprehensive the feature-maps extracted by  $D$  cover the information from the input images. This feature-extracting performance can be easily checked via an auto-encoding training. In detail, we take  $D$  trained in GAN and fix it, then train a decoder for  $D$  which tries to reconstruct the images from the feature-maps encoded by  $D$ . The intuition is, if  $D$  pays



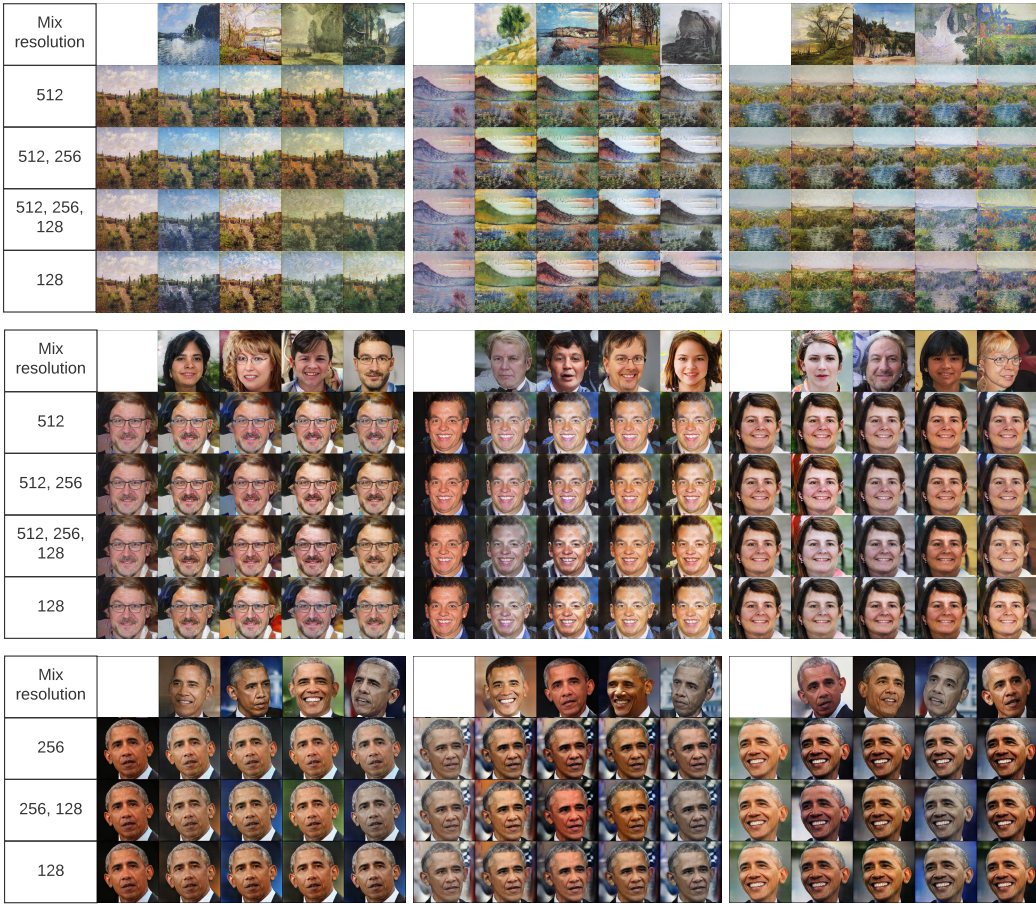
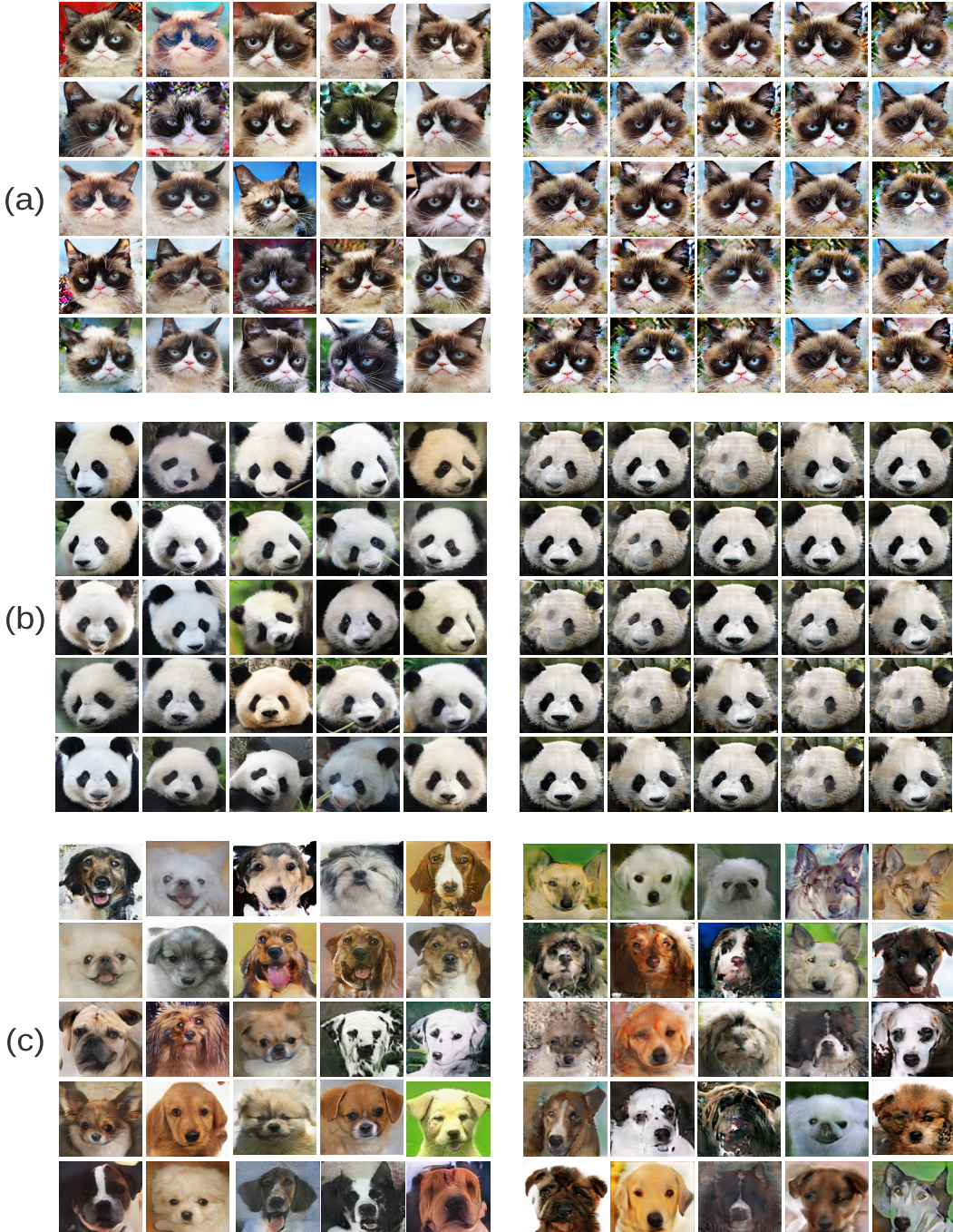
Figure 9: **Style-mixing results** by swapping the features for SLE on different resolutions.

Fig. 11 shows the results from the 1000 samples training on Art paintings and FFHQ at  $1024 \times 1024$  resolution, and the 100 samples Obama at  $256 \times 256$  resolution. In each row, we swap the  $x_{low}$  in the SLE layer from the image in col. 1 to the one from each image on row. 1. The best style-mixing results is achieved when the feature-map swapping is done on all resolutions. And the most effective layer that causes the most style changes is the layer on 128 resolution. On  $256 \times 256$  resolution, the model behaves the same, where the SLE on lower resolution makes the most style difference.

On the Art-paintings data, the model performs well on style-mixing, where not only the coloring but also the texture can be controlled. The models transfers the style of flat or pointy brush stroke among the style-mixed synthetic images. However, the model does not perform as well on the FFHQ data. There are some cases where even the hair color can not be properly transferred. We speculate that the worse performance on FFHQ is due to the limited training sample and the dramatically varied background. There is no clear relationship between the front-end face and the background contents given the limited training samples, which confuses the model to disentangle more detailed style attributes. In contrast, Art-paintings have consistent style cues within each image and obvious connections between each object inside a scene, making it arguably easier than the FFHQ data. On the other hand, the model performs great on Obama given a even less 100 training images. It successfully transfers the style for both the face attributes and the background. Learning on  $256^2$  resolution is a simpler task, and the model capacity is more sufficient on only 100 samples.

## D MORE QUALITATIVE COMPARISON



**Figure 10: Comparison between our model and the baseline** For each dataset, the images are generated by the same set of randomly sampled noises. Images from our model is shown on the left, and the baseline results are on the right. All the model are trained for 50000 iterations with batch size of 8, which is more than enough for both models to converge. On (a) Grumpy-cat and (b) Panda, baseline model shows a clear mode collapse, while our model is generating diverse images; on (c) Animalface-dog, although not mode collapse, the baseline model shows a clear quality disadvantage compared to our model.

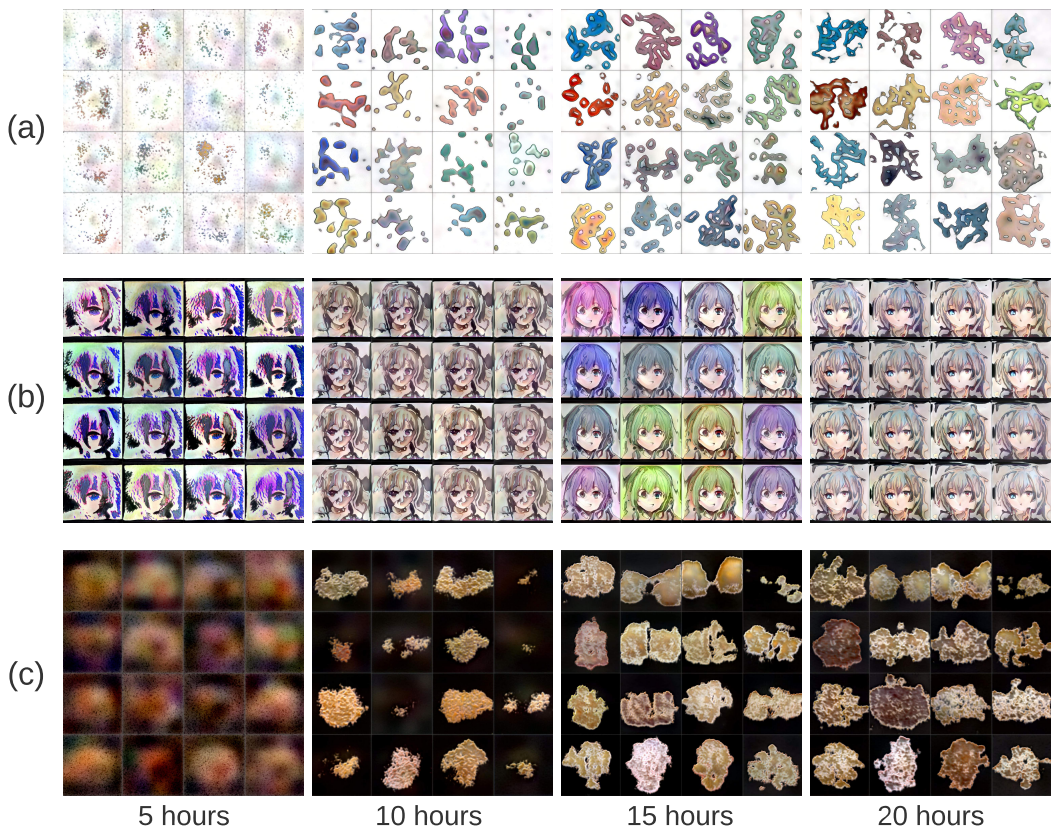
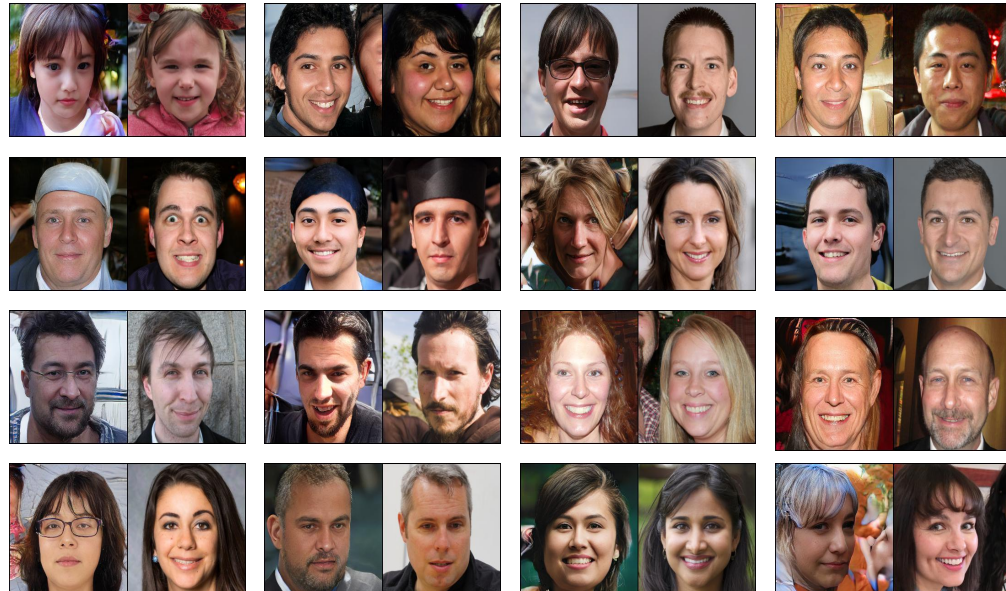


**Figure 11: StyleGAN2 results during training** We show the results of the slimed StyleGAN2 at half channel numbers. StyleGAN2 converges much slower than our model on dataset (a) Pokemon and (c) Shell, and mode collapsed on (b) Anime-Face.

## E NEAREST IMAGES FROM TRAINING SETS



(a) Art-paintings 1k



(b) FFHQ 1k

**Figure 12: Nearest real images to the synthesized ones trained on 1000 images** For each pair of images, the left is the synthesized image from our model, and the right image is the closest image found from the real training data ranked by LPIPS score. The samples are uncurated, and our model is able to create new contents that well fitted to the training domain.



**Figure 13: Nearest real images to the synthesized ones trained on 100 images** For each image pair, the left is the synthesized image from our model, and the right is the closest image found from the real training data ranked by LPIPS score. Even with only 100 training samples, these uncurated samples show our model is still able to combine the features learned from the real samples and synthesize new compositions.

Table 8: LPIPS between synthetic images and their closest real images.

	Art paintings 1k	FFHQ 1k	Skull	Cat	Dog	Shell
augmented	0.5499	0.5279	0.389	0.3898	0.3847	0.3853
Our G	0.637	0.5859	0.3168	0.5486	0.5647	0.4275

In Table 8, we report the average LPIPS score between the generated samples from our model to their closest real samples ranked by LPIPS score. In comparison, we show the baseline as the LPIPS between real images and their randomly augmented variants (randomly horizontal flipping and random cropping with 0.8 spatial portion). We run each experiment 3 times with 100 randomly synthesized samples or real images, and report the lowest one. The std among the trials are usually lower than 0.005. This experiment shows that, instead of memorizing the real images in the training set, our model is able to perceive the features from the real images, and generate images that are different and novel, in terms of compositions, shapes, and color patterns.

## F DECODER RESULT



Figure 14: **Reconstruction results from the decoder for training the auto-encoding discriminator.** For each dataset, the first panel shows the augmented real images during training, the second panel shows the reconstruction on full image, and the last panel shows the reconstruction on random cropped portions of the full image. All the reconstructions are done on  $128 \times 128$  resolution.

# FastGAN Summary

Improved GAN technique that can produce high quality output even with less training samples.  
Currently only on unconditional setting.

They propose a light-weight GAN structure that gains superior quality on  $1024 \times 1024$  resolution.  
Two techniques are used to achieve this, a skip-layer channel-wise excitation module and a self-supervised discriminator trained as a feature-encoder.

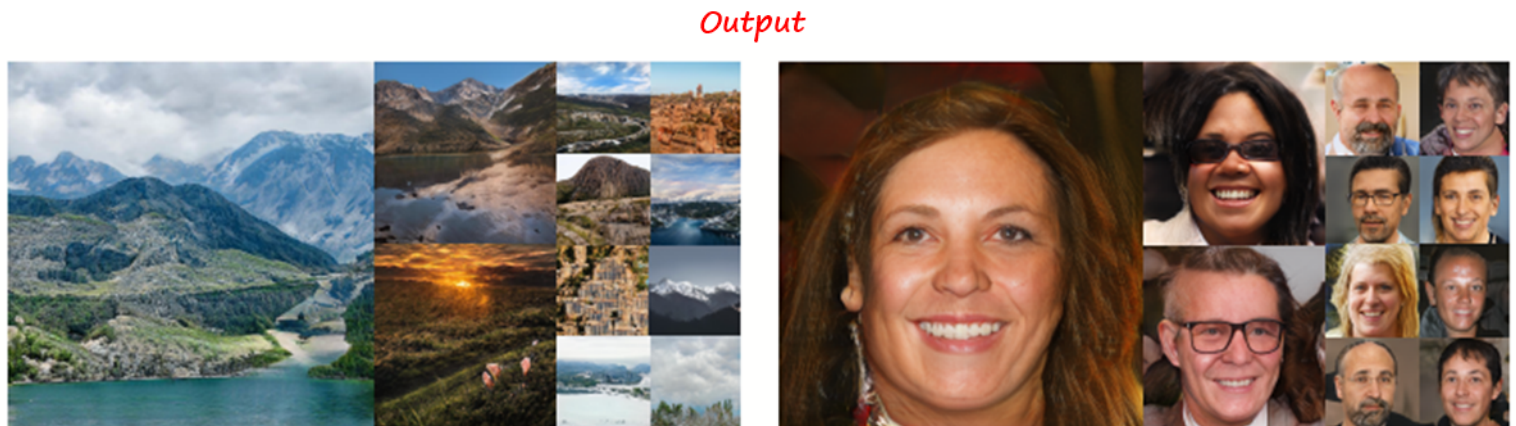


Figure 1: **Synthetic results on  $1024^2$  resolution** of our model, trained from scratch on single RTX 2080-Ti GPU, with only 1000 images. Left: 20 hours on Nature photos; Right: 10 hours on FFHQ.

## METHOD:

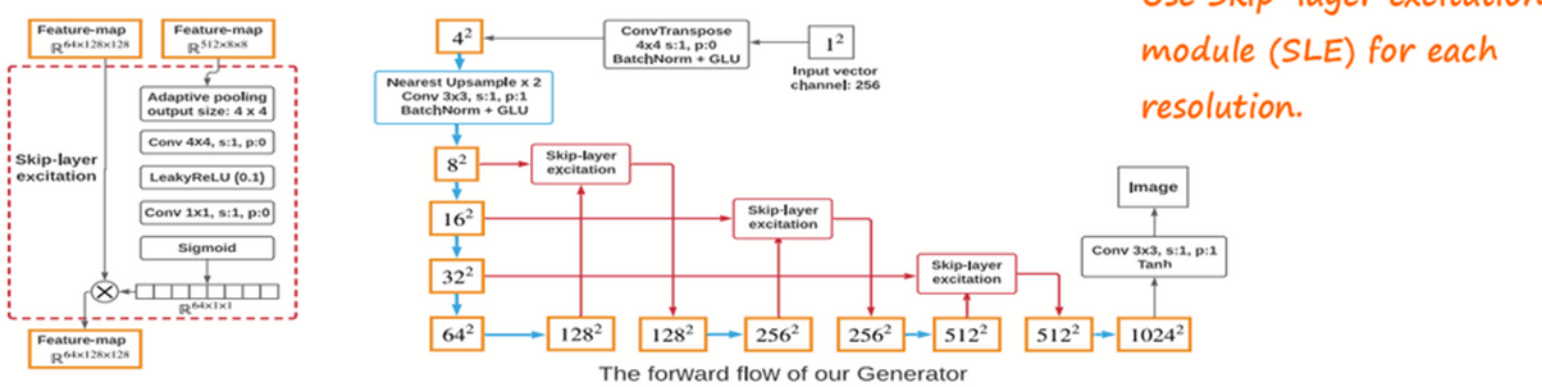


Figure 3: The structure of the skip-layer excitation module and the Generator. Yellow boxes represent feature-maps (we show the spatial size and omit the channel number), blue box and blue arrows represent the same up-sampling structure, red box contains the SLE module as illustrated on the left.

They reformulate the skip-connection idea with two unique designs into the Skip-Layer Excitation module (SLE). They use skip connections similar to ResNet but here they use  $1 \times 1$  convolution and multiplication instead of addition.  $1 \times 1$  convolution reduce number of parameters of model and multiplication reduce calculation overhead.

Formally, we define the Skip-Layer Excitation module as:

$$\mathbf{y} = \mathcal{F}(\mathbf{x}_{low}, \{\mathbf{W}_i\}) \cdot \mathbf{x}_{high} \quad (1)$$

Here  $\mathbf{x}$  and  $\mathbf{y}$  are the input and output feature-maps of the SLE module, the function  $\mathcal{F}$  contains the operations on  $\mathbf{x}_{low}$ , and  $\mathbf{W}_i$  indicates the module weights to be learned. The left panel in Fig. 3 shows an SLE module in practice, where  $\mathbf{x}_{low}$  and  $\mathbf{x}_{high}$  are the feature-maps at  $8 \times 8$  and  $128 \times 128$  resolution respectively. An adaptive average-pooling layer in  $\mathcal{F}$  first down-samples  $\mathbf{x}_{low}$  into  $4 \times 4$  along the spatial-dimensions, then a conv-layer further down-samples it into  $1 \times 1$ . A LeakyReLU is used to model the non-linearity, and another conv-layer projects  $\mathbf{x}_{low}$  to have the same channel size as  $\mathbf{x}_{high}$ . Finally, after a gating operation via a Sigmoid function, the output from  $\mathcal{F}$  multiplies  $\mathbf{x}_{high}$  along the channel dimension, yielding  $\mathbf{y}$  with the same shape as  $\mathbf{x}_{high}$ .

## SELF - SUPERVISED DISCRIMINATOR

Their approach to provide a strong regularization for  $D$  is straightforward. They treat  $D$  as an encoder and train it with small decoders.

The auto-encoding training forces  $D$  to extract image features that the decoders can give good reconstructions. The decoders are optimized together with  $D$  on a simple reconstruction loss, which is only trained on real samples:

$$\mathcal{L}_{recons} = \mathbb{E}_{\mathbf{f} \sim D_{encode}(x), x \sim I_{real}} [|||\mathcal{G}(\mathbf{f}) - \mathcal{T}(x)|||], \quad (2)$$

where  $\mathbf{f}$  is the intermediate feature-maps from  $D$ , the function  $\mathcal{G}$  contains the processing on  $\mathbf{f}$  and the decoder, and the function  $\mathcal{T}$  represents the processing on sample  $x$  from real images  $I_{real}$ .

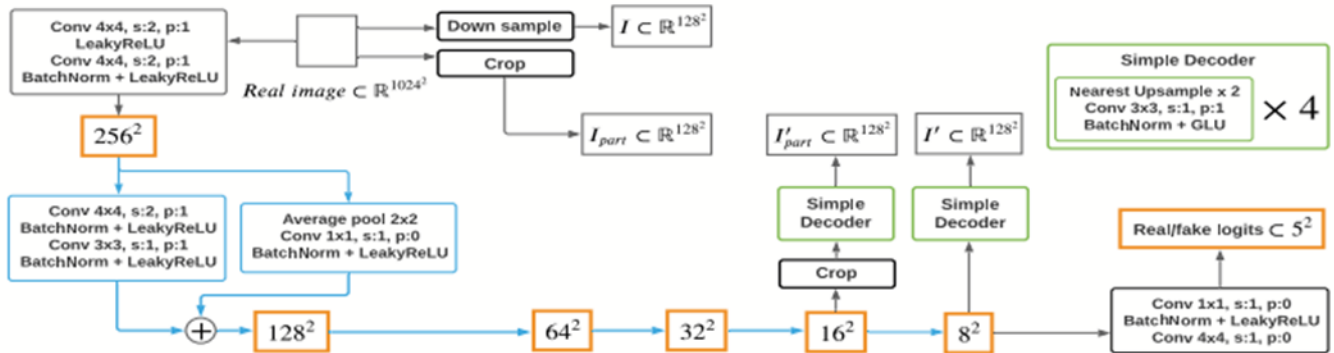


Figure 4: The structure and the forward flow of the Discriminator. Blue box and arrows represent the same residual down-sampling structure, green boxes mean the same decoder structure.

Their self-supervised D is illustrated in Fig. 4, where they employ two decoders for the feature-maps on two scales: f1 on 16x16 and f2 on 8x8 . The decoders only have four conv-layers to produce images at 128x128 resolution, causing little extra computations (much less than other regularization methods)

Such reconstructive training makes sure that D extracts a more comprehensive representation from the inputs, covering both the overall compositions and detailed textures.

### Loss Function:

Finally, they employ hinge version of adversarial loss to iteratively train D and G where they found hinge loss makes computation of GAN faster:

$$\mathcal{L}_D = - \mathbb{E}_{x \sim I_{real}} [\min(0, -1 + D(x))] - \mathbb{E}_{\hat{x} \sim G(z)} [\min(0, -1 - D(\hat{x})] + \mathcal{L}_{recons} \quad (3)$$

$$\mathcal{L}_G = - \mathbb{E}_{z \sim \mathcal{N}} [D(G(z))], \quad (4)$$